A Novel Discrete Particle Swarm Optimization for FRM FIR Digital Filters

Seyyed Ali Hashemi, Behrouz Nowrouzian
Department of Electrical and Computer Engineering, University of Alberta, Edmonton, AB, T6G-2V4, Canada
Email: {seyyedal, nowr}@ece.ualberta.ca

***Abstract*— This paper presents a novel discrete particle swarm optimization (PSO) for frequency response masking (FRM) finite impulse response (FIR) digital filters over the canonical signed-digit (CSD) multiplier coefficient space. A look-up table (LUT) scheme is employed to ensure that the PSO automatically searches through permissible CSD multiplier coefficient values in the course of optimization without any recourse to backtracking. This is achieved by searching through the indices of the CSD multiplier coefficient values in the LUT instead of the coefficient values themselves. In this way, the resulting multiplier coefficient values are ensured to conform to a prespecified wordlength as well as to a prespecified maximum number of non-zero digits. The salient feature of this LUT scheme is that by introducing barren layers in the LUT, there is no need to limit the search space manually in the course of PSO to prevent from going over the boundaries of the search space. Examples are given to illustrate the application of the proposed PSO to the design and optimization of a lowpass and a bandpass FRM FIR digital filters.**

***Index Terms*— Particle Swarm Optimization, Frequency Response Masking Approach, Digital Filters**

I. Introduction

DIGITAL filters find wide variety of applications in modern digital signal processing systems [1], [2]. The practical design of digital filters usually makes recourse to an optimization step en route to satisfying a given set of stringent design specifications. This optimization is usually carried out in terms of fixed configurations but variable multiplier coefficient values. In principle, there exist two different techniques available for the optimization of digital filters, namely, gradient-based and discrete optimization approaches. The desired coefficient values can readily be determined in infinite-precision by using hitherto optimization techniques. However, in an actual hardware implementation of the digital filters, the infinite-precision multipliers should be quantized to their finite-precision counterparts, but the resulting finite-precision multiplier coefficients may result in a digital filter that no longer satisfies the given design specifications. Consequently, from a hardware implementation point of view, there is every need for finite-precision optimization techniques.

There is a vast body of literature available for gradient-based optimization techniques, e.g. [3]–[7]. However, the large number of practical constraints usually involved in these techniques may adversely affect the computational efficiency of the optimization algorithm.

Simulated annealing (SA) [8] and genetic algorithms (GAs) [9], [10] have emerged as promising candidates for the design and *discrete* optimization of digital filters, particularly due to the fact that they are capable of automatically finding near-optimum solutions while keeping the computational complexity of the algorithm at moderate levels. They allow a robust search of the solution space through a parallel search in all directions without any recourse to gradient information.

particle swarm optimization (PSO) is an emerging attractive optimization technique. It was originally proposed by Kennedy and Eberhart in 1995 as a new intelligent optimization algorithm which simulates the migration and aggregation of a flock of birds seeking food [11]. It adopts a strategy based on particle swarm and parallel global random search, which may outperform other intelligent algorithms in computational speed and memory. In PSO, a potential candidate solution is represented as a particle in a multidimensional search space, where each dimension represents a distinct optimization variable. The particles in the multidimensional search space are characterized by corresponding fitness values. They make movements in the search space towards regions characterized by high fitness values.

This paper is concerned with the discrete PSO of a class of finite impulse response (FIR) digital filters. FIR digital filters are very attractive from a practical point of view because of their inherent stability features and simplicity of hardware implementation. However, the complexity of FIR digital filters is inversely proportional to their transition bandwidths, rendering them less economical if designed by using the classical techniques. Frequency response masking (FRM) technique is widely used for the design of computationally efficient sharp transition-band FIR digital filters [12]. Such narrow transition-bandwidth digital filters have many practical applications, e.g. in audio signal processing and data compression [13].

The starting point in the actual design of FRM FIR digital filters is to find the multiplier coefficient values constituent in the FIR digital filter in infinite-precision by using the hitherto gradient-based optimization techniques (e.g. Parks-McClellan approach [14]) followed by a quantization of the resulting coefficient values. The quantization can be performed by constraining the multiplier coefficients values to conform to certain number systems such as the signed power-of-two (SPT) system [15]. SPT is a computationally efficient number system

doi:10.4304/jcp.7.6.1289-1296

which can further reduce the hardware complexity of the FRM FIR digital filters. In this number system, each multiplier coefficient is represented to have only a few non-zero digits within its wordlength, permitting the decomposition of the multiplication operation into a finite series of shift and add operations. Digital filters incorporating SPT multiplier coefficient representation are commonly referred to as *multiplierless* digital filters [15]. However, the SPT representation of a given number is not unique, resulting in redundancy in the multiplier coefficient representation. This redundancy can adversely affect the corresponding computational complexity due to recourse to compare operations repetitively.

The canonical signed-digit (CSD) number system is a special case of the SPT number system which circumvents the above redundancy problem by limiting the number of non-zero digits in the representation of the multiplier coefficients. It is usually used in combination with subexpression sharing and elimination, which in turn results in substantial reduction in the cost of the hardware implementation of the digital filters [16]. In CSD number system, no two (or more) non-zero digits can appear consecutively in the representation of the multiplier coefficients, reducing the maximum number of non-zero digits by a factor of two in terms of shift and add operations [17].

After multiplier coefficient quantization, the resulting FRM FIR digital filter may no longer satisfy the given target design specifications. Therefore, the next step in the design of FRM FIR digital filters is to perform a further optimization to make the finite-precision FIR digital filter to conform to the design specifications. This can be achieved by resorting to a finite-precision optimization technique such as PSO. The proposed PSO involves a structural-level discrete optimization of FRM FIR digital filters in terms of actual CSD multiplier coefficient values, suitable for a direct hardware implementation.

A direct application of the conventional PSO algorithm to the optimization of the above FRM FIR digital filters gives rise to two separate problems. The first problem stems from the fact that in the course of optimization, PSO algorithm may lead to candidate FRM FIR digital filter particles whose multiplier coefficients values no longer conform to the CSD number format (due to random nature of velocity and position of particles). This problem is resolved by generating an indexed look-up table (LUT) of permissible CSD multiplier coefficient values, and by employing the indices of LUT to represent FRM FIR digital filter multiplier coefficient values. The indices of the LUT conform to the integer number format. Since the integer numbers are closed under the operations of addition and subtraction, PSO is made to search over the permissible CSD values in the LUT during the optimization process.

The second problem, on the other hand, stems from the fact that even in case of having an indexed LUT, the particles may go over the boundaries of the LUT in course of PSO due to the limited search space. This paper presents a new method to keep the particles inside the LUT in course of PSO without any recourse to backtracking, achieved by augmenting the LUT with *barren layers*. A barren layer is a region, with a certain width and certain entries, which is added to the problem space such that the particles tend to shy away from such a region. The width of the barren layers is calculated based on a worst case scenario that may happen in the particles movements in the search space. However, the entries of barren layers are different for different problems and depend on the topology of the search space and the fitness function used in the problem.

The remainder of this paper is organized as follows: Section II is concerned with a brief introduction to the conventional PSO algorithm. In Section III, the design of the FRM digital filter is reviewed. Section IV is concerned with the design of the bandpass FRM digital filters. Section V introduces the proposed novel discrete PSO for FRM FIR digital filters. In section VI, two examples are given to illustrate the application of the proposed PSO to the design and optimization of FRM FIR digital filters. Finally, section VII presents the main conclusions of the paper.

II. Conventional PSO Algorithm

Let us consider an optimization problem consisting of N design variables, and let us refer to each solution as a particle. Let us further consider a swarm of K particles in the N-dimensional search space. The position of the k-th particle in the search space can be assigned a N-dimensional position vector $X_k = \{x_{k1}, x_{k2}, \ldots, x_{kN}\}$. In this way, the element x_{kj} (for $j = 1, 2, \ldots, N$) represents the j-th coordinate of the particle X_k.

The PSO optimization fitness function maps each particle X_k in the search space to a fitness value. In addition, the particle X_k is assigned a N-dimensional velocity vector $V_k = \{v_{k1}, v_{k2}, \ldots, v_{kN}\}$. The PSO optimization search is directed towards promising regions by taking into account the velocity vector V_k together with the best previous position of the k-th particle $X_{best_k} = \{x_{best_{k1}}, x_{best_{k2}}, \ldots, x_{best_{kN}}\}$, and the best global position of the swarm $G_{best} = \{g_{best_1}, g_{best_2}, \ldots, g_{best_N}\}$ (i.e. the location of the particle with the best fitness value).

The conventional PSO is initialized by spreading the particles X_k through the search space in a random fashion. Then, the particles make movements through the search space towards regions characterized by high fitness values with corresponding velocities V_k. The movement of each particle is governed by the best previous location of the same particle X_{best_k}, and by the global best location G_{best}. The velocity of particle movement is determined from the previous best location of the particle, the global best location, and the previous velocity.

The velocity and position of each particle in the i-th iteration throughout the course of PSO are updated in accordance with Eqns. (1) and (2). In these equations, the parameter w represents an inertia weight; c_1 and c_2 are the correction (learning) factors, and r_1 and r_2 are random numbers in the interval $[0, 1]$. The velocity is limited between v_{min} and v_{max} to avoid very large

particle movements in the search space, where $v_{min} < 0$ and $v_{max} > 0$.

$$v_{kj}^{i} = wv_{kj}^{i-1} + c_1 r_1 (x_{best_{kj}}^{i-1} - x_{kj}^{i-1}) + c_2 r_2 (g_{best_j}^{i-1} - x_{kj}^{i-1}) \quad (1)$$

$$\text{if} \quad v_{kj}^{i} < v_{min} \quad ; \quad v_{kj}^{i} = v_{min}$$
$$\text{if} \quad v_{kj}^{i} > v_{max} \quad ; \quad v_{kj}^{i} = v_{max}$$
$$x_{kj}^{i} = x_{kj}^{i-1} + v_{kj}^{i} \quad (2)$$

The first term in the right hand side of movement update Eqn. (1), weighted by w, signifies the dependence of the current particle velocity on its value in the previous iteration. The second term, weighted by c_1, signifies an attractor to pull the particle towards its previous best position. The third term, weighted by c_2 controls the movement of the particle towards the global best position.

In addition to the update Eqns. (1) and (2), one can limit the coordinates in a particle between two user defined values $x_{j_{min}}$ and $x_{j_{max}}$ in order to limit the search space. However, This operation increases the complexity and consumes time.

III. Overview of FRM Digital Filter

The block diagram in Fig. 1 shows a conventional FRM digital filter, where $H_a(z)$ represents a FIR interpolation lowpass digital subfilter, and where $H_b(z)$ represents a power complementary counterpart of $H_a(z)$ in accordance with

$$|H_a(e^{j\omega})|^2 + |H_b(e^{j\omega})|^2 = 1 \quad (3)$$

Here, z represents the discrete-time complex frequency, and ω represents the corresponding (normalized) real frequency variable. Moreover, $F_0(z)$ and $F_1(z)$ represent FIR masking digital subfilters, while $H_a(z^M)$ and $H_b(z^M)$ represent M-fold interpolated versions of $H_a(z)$ and $H_b(z)$, respectively. The FRM digital filter in Fig. 1 has an overall transfer function

$$H(z) = H_a(z^M)F_0(z) + H_b(z^M)F_1(z) \quad (4)$$

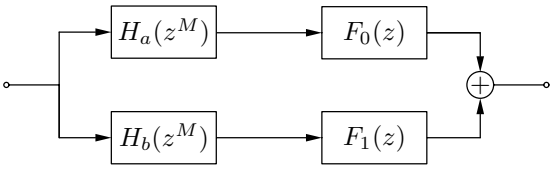

Figure 1. FRM Digital Filter Block Diagram

The masking digital subfilters $F_0(z)$ and $F_1(z)$ are employed to suppress the unwanted image bands produced by the interpolated digital subfilters $H_a(z^M)$ and $H_b(z^M)$. The corresponding interpolated digital subfilters $H_a(z^M)$ and $H_b(z^M)$ can realize transition bands which are a factor of M sharper than those of $H_a(z)$ and $H_b(z)$, without increasing the number of required non-zero digital multipliers. The magnitude frequency-response of the various subfilters incorporated by the FRM digital filter design approach are shown in Fig. 2.

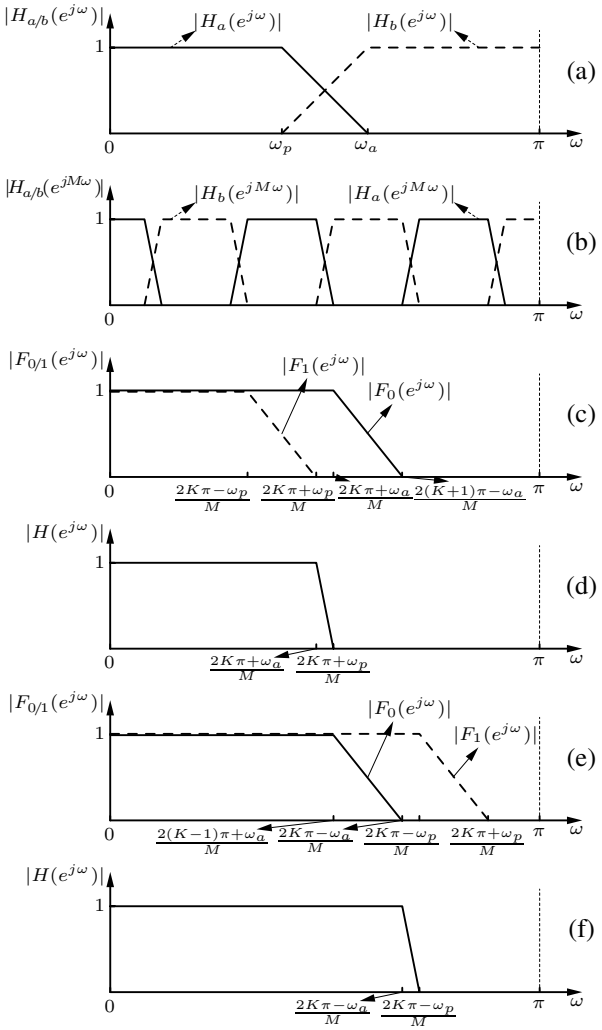

Figure 2. Magnitude Frequency-Response of FRM Digital Filter. (a) Magnitude Frequency-Response of the Bandedge-Shaping Digital Subfilters $H_a(z)$ and $H_b(z)$. (b) Magnitude Frequency-Response of the M-Interpolated Complementary Digital Subfilters $H_a(z^M)$ and $H_b(z^M)$. (c) Magnitude Frequency-Response of the Masking Digital Subfilters $F_0(z)$ and $F_1(z)$ for Case I. (d) Magnitude Frequency-Response of the Overall FRM Digital Filter $H(z)$ for Case I. (e) Magnitude Frequency-Response of the Masking Digital Subfilters $F_0(z)$ and $F_1(z)$ for Case II. (f) Magnitude Frequency-Response of the Overall FRM Digital Filter $H(z)$ for Case II [12].

IV. Design of Bandpass FRM Digital Filters

In general, it is possible to extend the conventional FRM approach for the design of bandpass or bandstop FRM digital filters. However, the resulting FRM digital filters are constrained to have identical lower and upper transition bandwidths. In [18], this restriction was relaxed by realizing the bandstop FRM FIR digital filter as a parallel combination of a corresponding pair of lowpass and highpass FIR digital filters. The latter lowpass and highpass FRM digital filters were obtained using a variation of the conventional FRM approach.

Let the desired bandpass FRM digital filter $H(z)$ have a lower transition bandwidth which is not identical to its upper transition bandwidth. $H(z)$ can be realized as a cascade combination of a pair of lowpass and highpass

FRM digital filters, so that

$$H(z) = H_{lp}(z)H_{hp}(z) \quad (5)$$

where $H_{lp}(z)$ represents a lowpass and $H_{hp}(z)$ represents a highpass FRM digital filter. In this way, $H_{lp}(z)$ and $H_{hp}(z)$ can be obtained with the help of Eqn. (4) as

$$H_{lp}(z) = H_{a_{lp}}(z^M)F_{0_{lp}}(z) + H_{b_{lp}}(z^M)F_{1_{lp}}(z) \quad (6)$$

$$H_{hp}(z) = H_{a_{hp}}(z^M)F_{0_{hp}}(z) + H_{b_{hp}}(z^M)F_{1_{hp}}(z) \quad (7)$$

The lower transition bandwidth is governed by the constituent transition bandwidth of the highpass FRM digital filter, while the upper transition bandwidth is governed by the constituent transition bandwidth of the lowpass FRM digital filter. The realization for bandpass FRM digital filter are as shown in Fig. 3.

V. Proposed discrete PSO for FRM FIR Digital Filters

The proposed discrete PSO of FRM FIR digital filters is carried out over the CSD multiplier coefficient space $CSD(L_0, l_0)$, where L_0 represents the multiplier coefficient wordlength, and where l_0 represents the maximum number of non-zero digits for FIR digital subfilters constituent in the FRM FIR digital filter. The multiplier coefficient values are taken from a CSD LUT which is constructed in a particular fashion.

A template LUT is constructed for all multiplier coefficient values for the interpolation digital subfilter $H_a(z)$ and the masking digital subfilters $F_0(z)$ and $F_1(z)$. The elements of this LUT belong to $CSD(L_0, l_0)$. The values of L_0 and l_0 are determined empirically based on the amplitude frequency-response of the digital subfilters $H_a(z)$, $F_0(z)$ and $F_1(z)$.

There are two problems concerning the PSO of FRM FIR digital filters over the CSD multiplier coefficient space. These two problems and the corresponding solutions are discussed in the following.

A. PSO indirect search method

In PSO, the required new particle position is obtained from the previous position of the particle through the addition of a random (normalized) velocity value. However, by directly applying the conventional PSO to the above optimization over the CSD multiplier coefficients, one may obtain new particle positions whose coordinate values are no longer in $CSD(L_0, l_0)$. In order to overcome this problem, the optimization search is carried out indirectly via the indices to the LUT CSD values (as opposed to LUT CSD values themselves). In this way, the CSD coordinate values for each particle position are obtained by integer indices to the CSD LUT. The key point in the indirect search rests with ensuring that the index set is closed, i.e. by ensuring that each index points to a valid CSD value in the LUT, and that the resulting particle in the course of PSO adheres to the prespecified CSD number format.

If the velocity values are replaced by their closest integer values, the update equations become modified to

$$\hat{v}_{kj}^i = [w\hat{v}_{kj}^{i-1} + c_1 r_1(\hat{x}_{best_{kj}}^{i-1} - \hat{x}_{kj}^{i-1}) + c_2 r_2(\hat{g}_{best_j}^{i-1} - \hat{x}_{kj}^{i-1})]^1 \quad (8)$$

$$\text{if} \quad \hat{v}_{kj}^i < \hat{v}_{min} \quad ; \quad \hat{v}_{kj}^i = \hat{v}_{min}$$

$$\text{if} \quad \hat{v}_{kj}^i > \hat{v}_{max} \quad ; \quad \hat{v}_{kj}^i = \hat{v}_{max}$$

$$\hat{x}_{kj}^i = \hat{x}_{kj}^{i-1} + \hat{v}_{kj}^i \quad (9)$$

Here, $\hat{x}_{kj}$, $\hat{v}_{kj}$, $\hat{x}_{best_{kj}}$, $\hat{g}_{best_j}$, $\hat{v}_{min}$ and $\hat{v}_{max}$ are all integer values where $\hat{v}_{min} < 0$ and $\hat{v}_{max} > 0$. In addition, w is limited in the interval $[0, 0.5)$ (to be discussed shortly).

In accordance with Eqn. (8), the velocity of a particle is an integer number. Since the integer number system is closed under the operations of addition and subtraction, Eqn. (9) assures PSO to search automatically over the CSD multiplier coefficient values in the LUT in an indirect fashion.

B. Barren layers

Due to its finite length, the template LUT inevitably confines the optimization to a bounded search space. In order to ensure that the particles do not cross over to the outside region of the search space in the course of PSO, the search space is constructed as a combination of two regions, namely the interior and barren layers. The barren layer is constructed to yield relatively low fitness values, and is represented as a header and footer in the template LUT. There are two problems concerning the construction of the barren layers:

1) barren layer entries: The first problem in the construction of barren layers concerns how to make the fitness values in the barren layer relatively low. This problem can be resolved by filling the header part by unrealistically large, and the footer part by unrealistically small CSD multiplier coefficient values. It should be noted that the barren layer entries are strongly dependant on the optimization problem at hand, i.e. the barren layer entries are different for different problems. In the FIR digital filter optimization applications, very large or very small multiplier coefficient values lead to candidate FRM FIR digital filters with relatively small fitness values. In this way, the particles are guaranteed to shy away from the resulting barren layers.

2) barren layer width: The second problem, on the other hand, concerns how to determine the width of the barren layer such that the particles do not cross over to the outside of the search space even under the worst case scenario. This problem relates to the number of entries in header and footer parts of the template LUT. To overcome this problem, let us consider the j-th variable in the k-th particle is in the boundaries of the template LUT in iteration $i-1$. The worst case scenario occurs when x_{kj}^{i-1} moves toward the barren layer with the peak permissible

[1] $[R]$ denotes rounding R to its closest integer, where R is assumed to be a real value.

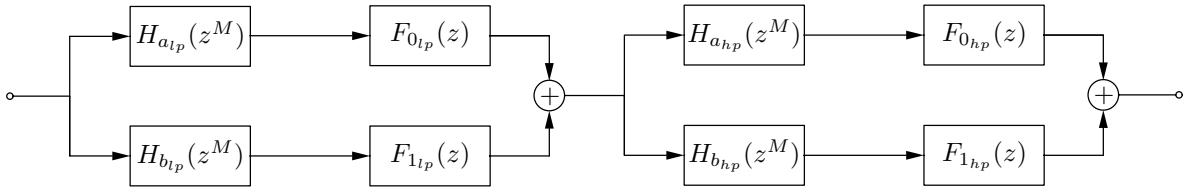

Figure 3. Bandpass FRM Digital Filter Block Diagram

velocities (v_{max} for the header, and v_{min} for the footer). If in the i-th iteration x_{kj}^i is in the footer:

$$\hat{x}_{best_{kj}}^i > \hat{x}_{kj}^i \tag{10}$$

$$\hat{g}_{best_j}^i > \hat{x}_{kj}^i \tag{11}$$

and if it is in the header:

$$\hat{x}_{best_{kj}}^i < \hat{x}_{kj}^i \tag{12}$$

$$\hat{g}_{best_j}^i < \hat{x}_{kj}^i \tag{13}$$

Eqns. (10)-(13) show that the velocity of the particle in iteration $i+1$ tends to move the particle in a direction opposite to the direction of the barren layers. Here, the worst case happens when $r_1 = r_2 = 0$. In this way, the number of entries L_f in the footer part, and the number of entries L_h in the header part are determined in accordance with

$$\begin{aligned} L_f &= |\hat{v}_{min}| + [w|\hat{v}_{min}|] + [w[w|\hat{v}_{min}|]] + \dots \\ &\le |\hat{v}_{min}| + \frac{|\hat{v}_{min}|}{2} + \frac{|\hat{v}_{min}|}{4} + \dots \\ &= 2|\hat{v}_{min}| \end{aligned} \tag{14}$$

$$\begin{aligned} L_h &= \hat{v}_{max} + [w\hat{v}_{max}] + [w[w\hat{v}_{max}]] + \dots \\ &\le \hat{v}_{max} + \frac{\hat{v}_{max}}{2} + \frac{\hat{v}_{max}}{4} + \dots \\ &= 2\hat{v}_{max} \end{aligned} \tag{15}$$

Let us recall that since $0 \le w < 0.5$,

$$\text{if} \quad v : \text{positive integer} \quad \Rightarrow \quad [wv] \le \frac{v}{2} \tag{16}$$

In addition, after some iterations $\hat{v}_{kj}^{i+1} = 0$. Otherwise, if $w \ge 0.5$, $\hat{v}_{kj}^{i+1}$ can never become zero, and the width of the barren layer will be infinity.

The augmented LUT remains fixed in the course of PSO, restricting automatic particle movement inside the limited search space. Modifying the index values constituent in each particle by adding the current indices to the length of the footer barren layer, L_f, discrete PSO algorithm is ready to optimize FRM FIR digital filters.

VI. Application Examples

This section is concerned with the application of the proposed PSO to the design and optimization of a pair of FRM FIR digital filters. One of these digital filters exhibits a lowpass while the other exhibits a bandpass magnitude frequency response. The design parameters for the discrete PSO of CSD FRM FIR digital filters are similar for both the examples and are as shown in Tables I and II.

[2] f_0 represents the number of bits in the fractional part.

TABLE I.
Discrete PSO Design Parameters

K	w	c_1	c_2	$\hat{v}_{min}$	$\hat{v}_{max}$	L_f	L_h
700	0.4	2	2	-5	5	10	10

TABLE II.
CSD Parameters

L_0	l_0	f_0[2]
12	3	7

A. Lowpass FRM FIR Digital Filter Design Example

This section is concerned with the design of a lowpass FRM FIR digital filter satisfying the magnitude response design specifications given in Table III over the CSD multiplier coefficient space.

TABLE III.
Design Specifications

Maximum Passband Ripple A_p	0.1[dB]
Minimum Stopband Loss A_a	40[dB]
Passband-Edge Normalized Frequency ω_p	0.60π[Rad]
Stopband-Edge Normalized Frequency ω_a	0.61π[Rad]
Normalized Sampling Period T	1[s]
Interpolation Factor M	6

The first step to design the FRM FIR digital filter is to find the length of the digital subfilters $H_a(z)$, $F_0(z)$ and $F_1(z)$. Given the design specification in Table III, The lengths of the digital subfilters $H_a(z)$, $F_0(z)$ and $F_1(z)$ are found to be 79, 24, and 42, respectively (based on Parks-McClellan approach), resulting in $N = 145$ The passband and stopband edge frequencies of the digital subfilters $H_a(z)$, $F_0(z)$ and $F_1(z)$ are determined by using the design equations given in [12]. Moreover, the passband ripple and stopband loss of these subfilters are set at 85% of the corresponding values given in the design specifications in Table III (in order to account for any second-order effects when using the design equations in [12]). In this way, the derived design specifications for the digital subfilters $H_a(z)$, $H_b(z)$, $F_0(z)$ and $F_1(z)$ are obtained as shown in Table IV.

Finally, by using Parks McClellan approach, the subfilters $H_a(z)$, $F_0(z)$ and $F_1(z)$ can be designed. Consequently, the magnitude frequency response of the overall infinite-precision lowpass FRM FIR digital filter $H(z)$ is obtained as shown in Fig. 4. Based on the infinite-precision lowpass FRM FIR digital filter, the correspond-

TABLE IV.
BAND-EDGE FREQUENCIES, PASSBAND RIPPLES AND STOPBAND LOSSES FOR DIGITAL SUBFILTERS $H_a(z)$, $H_b(z)$, $F_0(z)$ AND $F_1(z)$

Subfilter	Passband Edge Frequency	Stopband Edge Frequency	Passband Ripple	Stopband Loss
$H_a(z)$	0.34π	0.4π	0.085 dB	46 dB
$H_b(z)$	0.4π	0.34π	0.085 dB	46 dB
$F_0(z)$	0.4π	0.6π	0.085 dB	46 dB
$F_1(z)$	0.61π	0.723π	0.085 dB	46 dB

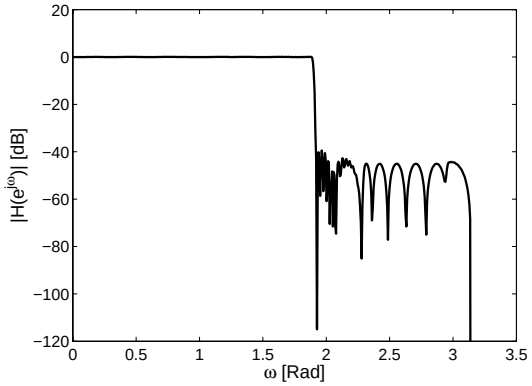

Figure 4. Magnitude Frequency-Response of the Overall Infinite-Precision Lowpass FRM FIR Digital Filter $H(e^{j\omega})$

ing CSD FRM FIR initial digital filter is obtained through rounding the infinite-precision multiplier coefficient values to their closest CSD values. The resulting CSD FRM FIR digital filter has a magnitude frequency response as shown in Fig. 5

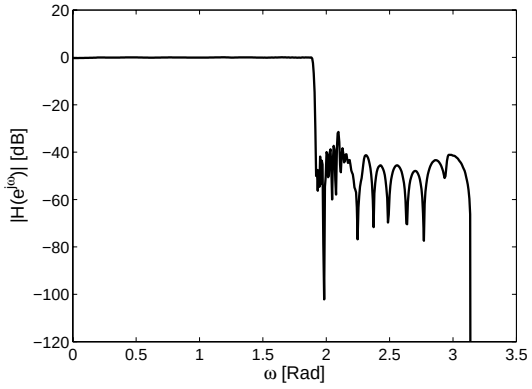

Figure 5. Magnitude Frequency-Response of the Overall Lowpass CSD FRM FIR Digital Filter $H(e^{j\omega})$ Before Discrete PSO

By applying the proposed discrete PSO to the above CSD FRM FIR digital filter and after about 100 iterations, the discrete PSO converges to the optimal lowpass FRM FIR digital filter having a magnitude frequency response as shown in Fig. 6. In addition, Fig. 7 gives us a closer look at the magnitude frequency response in the passband region of the lowpass FRM FIR digital filter.

Table V represents the comparison of the CSD lowpass FRM FIR digital filters before and after PSO.

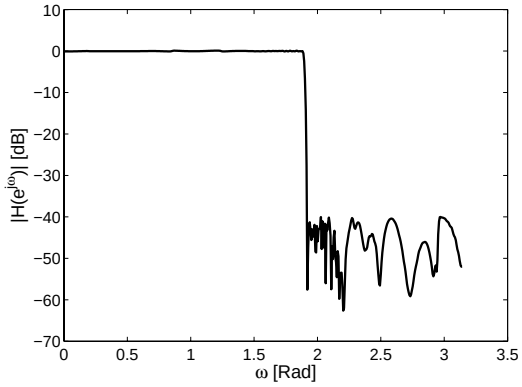

Figure 6. Magnitude Frequency-Response of the Overall Lowpass CSD FRM FIR Digital Filter $H(e^{j\omega})$ After Discrete PSO

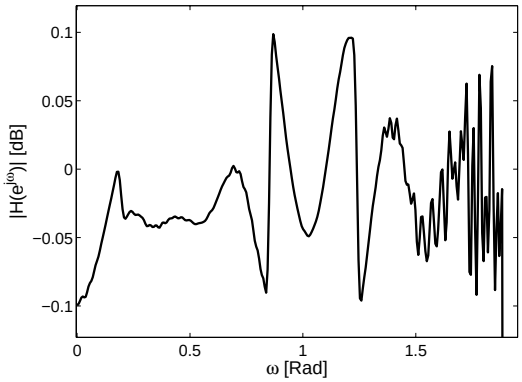

Figure 7. Magnitude Frequency-Response in the Passband Region of the Overall Lowpass CSD FRM FIR Digital Filter $H(e^{j\omega})$ After Discrete PSO

B. Bandpass FRM FIR Digital Filter Design Example

In this section, the design of a bandpass FRM FIR digital filter over the CSD multiplier coefficient space is considered. The given magnitude response design specifications are as given in Table VI.

As before, the first step to the design of the bandpass FRM FIR digital filter is to find the lengths of the digital subfilters $H_{a_{lp}}(z)$, $F_{0_{lp}}(z)$, $F_{1_{lp}}(z)$, $H_{a_{hp}}(z)$, $F_{0_{hp}}(z)$ and $F_{1_{hp}}(z)$. Using the design specifications given in Table VI, The lengths of the digital subfilters $H_{a_{lp}}(z)$, $F_{0_{lp}}(z)$ and $F_{1_{lp}}(z)$ are found to be 79, 24, and 42, respectively. Also, the lengths of the digital subfilters $H_{a_{hp}}(z)$, $F_{0_{hp}}(z)$ and $F_{1_{hp}}(z)$ are found to be 49, 23, and 35, respectively, resulting in $N = 252$. The passband ripple and stopband loss of these subfilters are set at 85% of the corresponding values given in Table VI. In this way, the derived design specifications for the digital subfilters $H_{a_{lp}}(z)$, $F_{0_{lp}}(z)$, $F_{1_{lp}}(z)$, $H_{a_{hp}}(z)$, $F_{0_{hp}}(z)$ and $F_{1_{hp}}(z)$ are obtained as shown in Table VII.

Finally, by using Parks McClellan approach, the subfilters $H_{a_{lp}}(z)$, $F_{0_{lp}}(z)$, $F_{1_{lp}}(z)$, $H_{a_{hp}}(z)$, $F_{0_{hp}}(z)$ and $F_{1_{hp}}(z)$ can be designed. The magnitude frequency response of the overall infinite-precision bandpass FRM FIR digital filter $H(z)$ is as shown in Fig. 8.

TABLE V.
FREQUENCY-RESPONSE ANALYSIS OF THE LOWPASS CSD FRM FIR DIGITAL FILTER BEFORE AND AFTER DISCRETE PSO

Frequency-Response Characteristic	Before Discrete PSO	After Discrete PSO
Maximum Passband Ripple A_p	0.2788[dB]	0.0996[dB]
Minimum Stopband Loss A_a	31.4681[dB]	40.0269[dB]

TABLE VI.
DESIGN SPECIFICATIONS

Maximum Passband Ripple A_p	0.1[dB]
Minimum Stopband Loss A_a	40[dB]
Lower Stopband-Edge Normalized Frequency ω_{a_1}	0.31π[Rad]
Lower Passband-Edge Normalized Frequency ω_{p_1}	0.33π[Rad]
Upper Passband-Edge Normalized Frequency ω_{p_2}	0.60π[Rad]
Upper Stopband-Edge Normalized Frequency ω_{a_2}	0.61π[Rad]
Normalized Sampling Period T	1[s]
Lowpass Filter Interpolation Factor M_{lp}	6
Highpass Filter Interpolation Factor M_{hp}	5

TABLE VII.
BAND-EDGE FREQUENCIES, PASSBAND RIPPLES AND STOPBAND LOSSES FOR DIGITAL SUBFILTERS $H_{a_{lp}}(z)$, $H_{b_{lp}}(z)$, $F_{0_{lp}}(z)$, $F_{1_{lp}}(z)$, $H_{a_{hp}}(z)$, $H_{b_{hp}}(z)$, $F_{0_{hp}}(z)$ AND $F_{1_{hp}}(z)$

Subfilter	Passband Edge Frequency	Stopband Edge Frequency	Passband Ripple	Stopband Loss
$H_{a_{lp}}(z)$	0.34π	0.4π	0.085 dB	46 dB
$H_{b_{lp}}(z)$	0.4π	0.34π	0.085 dB	46 dB
$F_{0_{lp}}(z)$	0.4π	0.6π	0.085 dB	46 dB
$F_{1_{lp}}(z)$	0.61π	0.723π	0.085 dB	46 dB
$H_{a_{hp}}(z)$	0.35π	0.45π	0.085 dB	46 dB
$H_{b_{hp}}(z)$	0.45π	0.35π	0.085 dB	46 dB
$F_{0_{hp}}(z)$	0.31π	0.09π	0.085 dB	46 dB
$F_{1_{hp}}(z)$	0.47π	0.33π	0.085 dB	46 dB

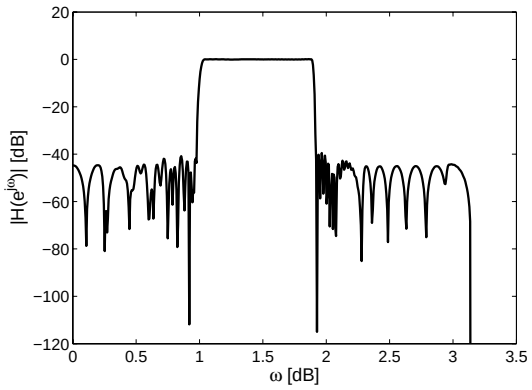

Figure 8. Magnitude Frequency-Response of the Overall Infinite-Precision Bandpass FRM FIR Digital Filter $H(e^{j\omega})$

Based on the infinite-precision bandpass FRM FIR digital filter, the corresponding CSD FRM FIR digital filter is obtained to have a magnitude frequency response as shown in Fig. 9

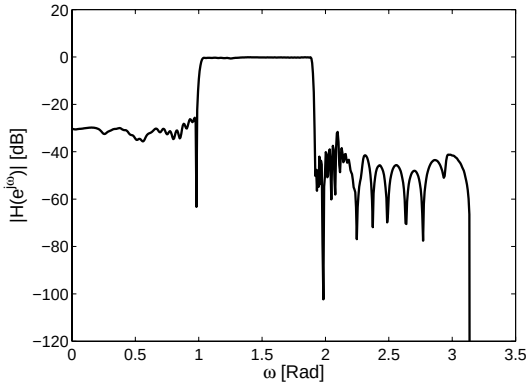

Figure 9. Magnitude Frequency-Response of the Overall Bandpass CSD FRM FIR Digital Filter $H(e^{j\omega})$ Before Discrete PSO

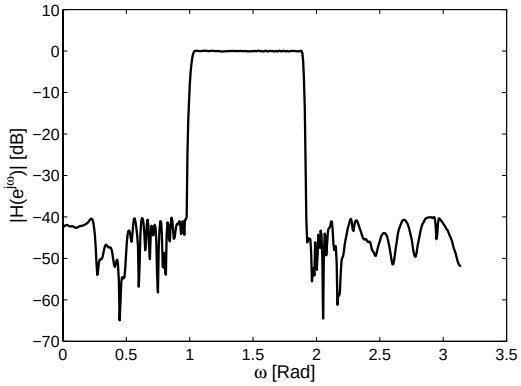

Figure 10. Magnitude Frequency-Response of the Overall Bandpass CSD FRM FIR Digital Filter $H(e^{j\omega})$ After Discrete PSO

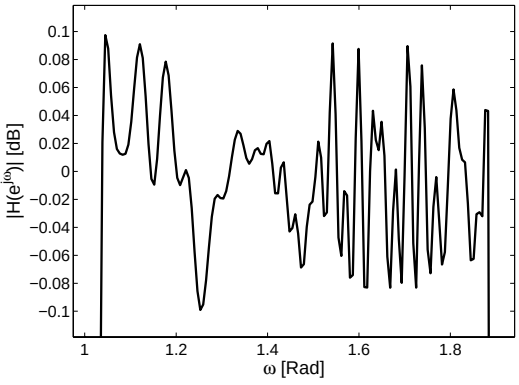

Figure 11. Magnitude Frequency-Response in the Passband Region of the Overall Bandpass CSD FRM FIR Digital Filter $H(e^{j\omega})$ After Discrete PSO

By applying the proposed discrete PSO to the above CSD FRM FIR digital filter and after about 200 iterations, the discrete PSO converges to the optimal bandpass FRM FIR digital filter having a magnitude frequency response as shown in Fig. 10. Fig. 11 gives us a closer look at the magnitude frequency response in the passband region of the bandpass FRM FIR digital filter.

Table VIII compares the CSD bandpass FRM FIR

TABLE VIII.
FREQUENCY-RESPONSE ANALYSIS OF THE BANDPASS CSD FRM FIR DIGITAL FILTER BEFORE AND AFTER DISCRETE PSO

Frequency-Response Characteristic	Before Discrete PSO	After Discrete PSO
Maximum Passband Ripple A_p	0.6277[dB]	0.0991[dB]
Minimum Stopband Loss A_a	25.6378[dB]	40.0125[dB]

digital filters before and after discrete PSO.

VII. CONCLUSION

This paper has presented a novel CSD LUT-based technique for the design and optimization of FRM FIR digital filters by employing discrete particle swarm optimization (PSO). By augmenting the LUT with barren layers, the CSD FRM FIR digital filters generated in the course of PSO are guaranteed to remain automatically within the CSD LUT boundaries without any recourse to backtracking. Moreover, by performing PSO on the indices of CSD values in the LUT (as opposed to the CSD values themselves), the wordlength and the maximum number of non-zero digits in the CSD multiplier coefficients remain fixed automatically throughout the course of PSO. In this way, the candidate FRM FIR digital filters generated in the course of PSO conform to a prespecified CSD multiplier coefficient wordlength and to a prespecified maximum number of non-zero CSD digits. The usefulness of the proposed PSO algorithm has been illustrated through its application to the design of a lowpass and a bandpass FRM FIR digital filter satisfying stringent design specifications.

REFERENCES

[1] D. R. Wilson, D. R. Corrall, and R. F. Mathias, "The Design and Application of Digital Filters," *IEEE Transactions on Industrial Electronics and Control Instrumentation*, vol. IECI-20, pp. 68–74, 1973.

[2] P. P. Vaidyanathan, "Multirate digital filters, filter banks, polyphase networks, and applications: a tutorial," *Proceedings of the IEEE*, vol. 78, pp. 56–93, 1990.

[3] Y. Lim, S. Parker, and A. Constantinides, "Finite Word Length FIR Filter Design Using Integer Programming over a Discrete Coefficient Space," *IEEE Transactions on Acoustics, Speech and Signal Processing*, vol. 30, pp. 661–664, 1982.

[4] T. Saramaki and Y. C. Lim, "Use of the Remez Algorithm for Designing FIR Filters Utilizing the Frequency-Response Masking Approach," in *1999 IEEE International Symposium on Circuits and Systems. ISCAS '99*, vol. 3, 1999, pp. 449–455.

[5] Y. J. Yu and Y. C. Lim, "FRM Based FIR Filter Design - the WLS Approach," in *2002 IEEE International Symposium on Circuits and Systems. ISCAS 2002*, vol. 3, 2002, pp. III–221 – III–224.

[6] W.-S. Lu and T. Hinamoto, "Optimal Design of Frequency-Response-Masking Filters Using Semidefinite Programming," *IEEE Transactions on Circuits and Systems I: Fundamental Theory and Applications*, vol. 50, pp. 557–568, 2003.

[7] ——, "Optimal Design of FIR Frequency-Response-Masking Filters Using Second-Order Cone Programming," vol. 3, 2003, pp. III–878 – III–881.

[8] L. Cen and Y. Lian, "Hybrid Genetic Algorithm for the Design of Modified Frequency-Response Masking Filters in a Discrete Space," *Circuits, Systems, and Signal Processing*, vol. 25, pp. 153–174, April 2006.

[9] P. Mercier, S. M. Kilambi, and B. Nowrouzian, "Optimization of FRM FIR Digital Filters Over CSD and CDBNS Multiplier Coefficient Spaces Employing a Novel Genetic Algorithm," *Journal of Computers*, vol. 2, no. 7, pp. 20–31, Sept. 2007.

[10] S. Bokhari and B. Nowrouzian, "DCGA Optimization of Lowpass FRM IIR Digital Filters Over CSD Multiplier Coefficient Space," in *52nd IEEE International Midwest Symposium on Circuits and Systems*, August 2009.

[11] J. Kennedy and R. Eberhart, "Particle Swarm Optimization," in *Proceedings of IEEE International Conference on Neural Networks*, vol. 4, 1995, pp. 1942–1948.

[12] Y. Lim, "Frequency-Response Masking Approach for the Synthesis of Sharp Linear Phase Digital Filters," *IEEE Transactions on Circuits and Systems*, vol. 33, no. 4, pp. 357–364, 1986.

[13] ——, "A Digital Filter Bank for Digital Audio Systems," *IEEE Transactions on Circuits and Systems*, vol. 33-8, p. 848 849, Aug. 1986.

[14] T. Parks and J. McClellan, "Chebyshev Approximation for Nonrecursive Digital Filters with Linear Phase," *IEEE Transactions on Circuit Theory*, vol. CT-19, pp. 189–194, 1972.

[15] Y. C. Lim, R. Yang, D. Li, and J. Song, "Signed Power-of-Two Term Allocation Scheme for the Design of Digital Filters," *IEEE Transactions on Circuits and Systems II: Analog and Digital Signal Processing*, vol. 46, pp. 577–584, 1999.

[16] R. I. Hartley, "Subexpression Sharing in Filters Using Canonic Signed Digit Multipliers," *IEEE Transactions on Circuits and Systems II: Analog and Digital Signal Processing*, vol. 43, pp. 677–688, 1996.

[17] A. T. G. Fuller, B. Nowrouzian, and F. Ashrafzadeh, "Optimization of FIR Digital Filters over the Canonical Signed-Digit Coefficient Space Using Genetic Algorithms," in *1998 Midwest Symposium on Circuits and Systems*, 1998, pp. 456–459.

[18] R. Yang, Y.-C. Lim, and S. R. Parker, "Design of sharp linear-phase FIR bandstop filters using the frequency-response-masking technique," *Circuits, Systems, and Signal Processing*, vol. 17, no. 1, pp. 1–27, Jan. 1998.

Seyyed Ali Hashemi received his M.Sc. degree in electrical engineering from University of Alberta, Edmonton, Alberta, Canada, in 2011. He received his B.Sc. degree in electrical engineering from Sharif University of Technology, Tehran, Iran, in 2009. His research interests include the design and optimization of digital circuits and systems.

Behrouz Nowrouzian received the B.Sc. degree in electrical engineering from Arya-Mehr (Sharif) University of Technology, Tehran, Iran, in 1975. He received the M.Sc., D.I.C., and Ph.D. degrees from the Imperial College of Science and Technology, University of London, London, U.K, in 1976, 1977, and 1983, respectively.

He was a member of Micronet, a network funded by Industry and the Federal Government of Canada of Excellence (NCE) program from 1991 to 2005.

Currently, he is a Professor at the Department of Electrical and Computer Engineering, University of Alberta, Edmonton, Alberta, Canada. His main research interests include VLSI digital signal processing, computer arithmetic and architecture, high-level-synthesis, and optimization of circuits and systems.